NOX4 aggravates doxorubicin-induced cardiomyocyte pyroptosis by increasing reactive oxygen species content and activating the NLRP3 inflammasome

Hong Zeng[1], Pengtao Zou[1], Yanmei Chen[1], Ping Zhang[2], Liang Shao[1]

[1]Department of Cardiology, Jiangxi Provincial People's Hospital, the First Affiliated Hospital of Nanchang Medical College, Nanchang, China; [2]Department of Neurology, Jiangxi Provincial People's Hospital, the First Affiliated Hospital of Nanchang Medical College, Nanchang, China

Contributions: (I) Conception and design: H Zeng; (II) Administrative support: H Zeng, L Shao; (III) Provision of study materials or patients: H Zeng, P Zou, Y Chen; (IV) Collection and assembly of data: H Zeng, P Zou, Y Chen; (V) Data analysis and interpretation: H Zeng, L Shao, P Zhang; (VI) Manuscript writing: All authors; (VII) Final approval of manuscript: All authors.

Correspondence to: Liang Shao, MD. Department of Cardiology, Jiangxi Provincial People's Hospital, the First Affiliated Hospital of Nanchang Medical College, No. 92, Aiguo Rd., Donghu District, Nanchang 330006, China. Email: shaoliang5201@126.com.

Background: Nicotinamide adenine dinucleotide phosphate oxidase 4 (NOX4)-mediated reactive oxygen species (ROS) has been reported to induce cardiomyocyte apoptosis, but its effect on pyroptosis of cardiomyocytes has been rarely reported. This paper aimed to explore the effects of NOX4-mediated ROS production on doxorubicin (DOX)-induced myocardial injury and pyroptosis through nucleotide-binding and oligomerization domain-like receptor protein 3 (NLRP3) inflammasome.

Methods: HL-1 cells were treated with DOX or mice (30 mice were divided into five groups with six mice/group) underwent intraperitoneal injection with DOX (5 mg/kg, once a week, five times) to induce myocardial injury, followed by assessment of NOX4 and NLRP3 expression in cell supernatant and myocardial tissues. In cardiomyocyte HL-1 cells, cell proliferation was tested by MTT assay and the activity of ROS by probes. The superoxide dismutase (SOD) activity, malondialdehyde (MDA) content, and glutathione (GSH) activity were evaluated by kits. The expression of pyroptosis proteins was assessed by western blotting. Subsequently, the expression of NOX4 or NLRP3 was altered to determine the effect of NOX4 or NLRP3 expression on cardiomyocyte injury and pyroptosis. The animal models were utilized to evaluate the changes in the cardiac function of mice using an echocardiographic system, with these parameters measured including left ventricular ejection fraction (LVEF), left ventricular fractional shortening (LVFS), and left ventricular end-diastolic diameter (LVEDD). Furthermore, the content of myocardial injury markers and the protein expression of pyroptosis proteins were determined to evaluate myocardial injury in the mice.

Results: DOX treatment led to cardiomyocyte injury and pyroptosis, as evidenced by weakened LVEF, LVFS, and cell proliferation (P<0.05), elevated LVEDD, ROS, and MDA (P<0.05), increased expression of pyroptosis proteins (P<0.05), and decreased SOD and GSH (P<0.05). Additionally, NOX4 and NLRP3 were highly-expressed (P<0.05) in cell supernatant and myocardial tissues. In DOX-induced HL-1 cells, the overexpression of NOX4 intensified ROS levels to aggravate cardiomyocyte injury and pyroptosis, which was reversed by treatment of the ROS scavenger N-acetyl-cysteine. Furthermore, it was revealed that the combination of short hairpin RNA (sh)-NOX4 and overexpressed (oe)-NLRP3 reversed the cardioprotective effects of sh-NOX4 and increased myocardial tissue or cell injury and pyroptosis *in vitro* and *in vivo*. No mice died during the animal experiments, and only two were ruled out due to a weight loss greater than 20%.

Conclusions: NOX4-mediated ROS production activated NLRP3 inflammasome, thereby aggravating DOX-induced myocardial injury *in vitro* and *in vivo*.

Keywords: Nicotinamide adenine dinucleotide phosphate oxidase 4 (NOX4); reactive oxygen species (ROS); nucleotide-binding and oligomerization domain-like receptor protein 3 (NLRP3); myocardial injury; pyroptosis

Introduction

Doxorubicin (DOX) is a widely used and effective antibiotic for the treatment of a variety of carcinomas (1). However, its clinical application is significantly limited due to its cumulative and dose-dependent cardiotoxicity, which can further develop into irreversible myocardial injury and eventually lead to congestive heart failure (2). Pyroptosis and oxidative stress are considered to be two major factors in the development of DOX-induced cardiomyopathy (3,4). Unfortunately, there are limited recognized treatments for myocardial injury caused by DOX, and none of them has achieved completely satisfactory results (5). In light of this, it is imperative to investigate the molecular mechanisms underlying myocardial injury and pyroptosis to promote the treatment of DOX-induced myocardial injury.

Pyroptosis is a programmed cell death, demonstrating a proinflammatory effect, which is linked with inflammasome activation (6). A prior study has shown that the pyroptosis process is mainly regulated by caspases and gasdermin D (GSDMD) proteins (7). Specifically, nucleotide-binding and oligomerization domain-like receptor (NLR) is activated by inflammatory stimulation, followed by the combination with pro-caspase-1. The activated caspase-1 further shears GSDMD (a member of the GSDM protein family consisting of more than 500 amino acids), and the obtained GSDMD-N terminal can accumulate on the cell membrane and cause cell membrane perforation and release of inflammatory factors, eventually leading to cell death (8). Nucleotide-binding and oligomerization domain-like receptor protein 3 (NLRP3) is currently the most thoroughly studied inflammasome. For instance, Zeng *et al.* demonstrated that NLRP3 inflammasome-mediated pyroptosis participated in the myocardial dysfunction progression and dilated cardiomyopathy pathogenesis (9).

Nicotinamide adenine dinucleotide phosphate (NADPH) oxidase 4 (NOX4) mainly functions in catalyzing the reduction of oxygen to superoxide anion and is one of the main sources of reactive oxygen species (ROS) within cells (10). A previous study revealed that echinacoside decreased ROS content by inhibiting NOX4 and ultimately inhibited cardiomyocyte pyroptosis and improved heart function (11), which demonstrated that NOX4-induced ROS accumulation exerted a regulatory role in programmed cell death. NOX4 also has been reported to play a vital role in NLRP3/caspase-1-dependent pyroptosis of H9c2 cardiomyoblasts (12). ROS occupies a vital position in the regulation of pyroptosis, and many chemicals activate NLRP3 inflammasome by increasing intracellular ROS content (13,14). A ROS inhibitor, N-acetyl-cysteine (NAC) could block the activation of NLRP3 to inhibit pyroptosis (15).

Building upon these findings, we put forward a hypothesis: in DOX-induced cardiomyocyte injury, NOX4 can mediate ROS accumulation and activate NLRP3 inflammasome to promote pyroptosis. Consequently, this study was designed to verify this hypothesis in an attempt to provide a new insight into the pathogenic mechanism that underlies myocardial injury triggered by DOX. We present this article in accordance with the ARRIVE reporting checklist (available at https://cdt.amegroups.com/article/view/10.21037/cdt-23-142/rc).

Highlight box

Key findings

- This paper found that nicotinamide adenine dinucleotide phosphate oxidase 4 (NOX4)-mediated reactive oxygen species (ROS) production activated nucleotide-binding and oligomerization domain-like receptor protein 3 (NLRP3) inflammasome, thereby aggravating doxorubicin (DOX)-induced myocardial injury *in vitro* and *in vivo*.

What is known and what is new?

- Pyroptosis and oxidative stress are considered to be two major factors in the development of DOX-induced cardiomyopathy. NOX4-mediated ROS has been reported to induce cardiomyocyte apoptosis, but its effect on pyroptosis of cardiomyocytes has been rarely reported.
- Our results showed that NOX4 and NLPR3 were increased in DOX-treated HL-1 cells, and NOX4-mediated ROS production regulates cardiomyocyte injury via NLPR3.

What is the implication, and what should change now?

- This work confirmed that the knockdown of NOX4 alleviated myocardial injury and pyroptosis following DOX induction through ROS/NLRP3 inflammasome signaling pathway, providing potential clinical therapeutic targets for reducing DOX-induced myocardial injury.

Methods

Cell culture

To ensure the species homology between cells and animal experiments, the results of mutual verification between cells *in vitro* and animals *in vivo* were considered as a whole. With reference to previous study (16), we used mouse HL-1 cardiomyocytes and C57BL/6J mice for experiments. HL-1 cells (iCell-m077, iCell Bioscience, Shanghai, China) were cultured in DMEM-high glucose (Gibco, Grand Island, NY, USA) supplemented with 1% penicillin/streptomycin and 10% fetal bovine serum. Once HL-1 cells had reached 80% confluence, the cells were separated by 0.25% trypsin-EDTA (Gibco) in phosphate-buffered saline (PBS) and neutralized with fresh medium. Next, the cell suspension was centrifuged at 1,200 rpm for 5 min. HL-1 cells were cultured under the conditions of 5% CO_2 and 37 ℃. The medium was changed every 3 days.

Cell injury induction

At 70% confluence, HL-1 cells were rinsed twice with serum-free medium, before exposure to different concentrations of DOX (0, 1, 2, 5, 10 µmol/L) for 24 h (17,18). DOX (purchased form Sigma-Aldrich, St. Louis, MO, USA) was dissolved in water and stored in a refrigerator at 4 ℃.

Cell transfection

NOX4 overexpression vector (oe-NOX4) (NOX4 fell-length CDS sequence), short hairpin RNA (sh)-NOX4 (sequence: CCTACGCAATAAGAGTTTCTA), NLRP3 overexpression vector (oe-NLRP3) (NLRP3 fell-length CDS sequence), and their negative controls [oe-NC, sh-NC, and oe-NC (sequence of sh-NC: TTGAACACTGGTGCGCCAGCT)] were procured from Hanbio Biotechnology Co., Ltd. (Shanghai, China) and then transfected into HL-1 cells for 48 h using Lipo3000 kit (Invitrogen, Carlsbad, CA, USA) according to the instructions. The concentration of the transfection vector was 100 nM (19). The transfection efficiency was determined by detecting gene expression.

Cells were grouped into control and DOX groups (cells were treated with 5 µmol/L DOX). Cells in the DOX group received different treatments according to the following groups: oe-NOX4 group (cells were transfected with oe-NOX4 and then treated with DOX), oe-NC group (served as the control for the oe-NOX4 group), sh-NOX4 group (cells were transfected with sh-NOX4 and then treated with DOX), sh-NC group (served as the control for the sh-NOX4 group), oe-NOX4 + NAC group [5 mM (20), cells were transfected with oe-NOX4 and then treated with NAC, followed by DOX treatment 1 h later], oe-NOX4 + dimethylsulfoxide (DMSO, the vehicle for NAC; Sigma-Aldrich) group (served as the control for the oe-NOX4 + NAC group), oe-NC + DMSO group (served as the control for the oe-NOX4 + DMSO group), sh-NOX4 + oe-NLRP3 group (cells were transfected with sh-NOX4 + oe-NLRP3 and then treated with DOX), sh-NOX4 + oe-NC group (served as the control for the sh-NOX4 + oe-NLRP3 group), and sh-NC + oe-NC group (served as the control for the sh-NOX4 + oe-NC group).

3-(4,5-dimethylthiazol-2-yl)-2,5-diphenyltetrazolium bromide (MTT) assay

After cells were planted onto 96-well plates, each well was treated with 10 µL of MTT solution (M6494, Thermo Fisher Scientific, Waltham, MA, USA) for 2 h. Three replicate wells were set for each sample. Finally, DMSO was utilized to stop the reaction and a microplate reader (model 680; Bio-rad, Hercules, CA, USA) was used to measure absorbance at 490 nm. Each assay was repeated thrice.

Immunofluorescence (IF)

Transfected cells were digested, counted, and incubated in IF chambers with 2×10^5 cells per well. When 60–80% confluence was reached, cells were washed with PBS (3×5 min) and fixed in 4% paraformaldehyde for 15 min, followed by additional PBS washing (3×5 min). Next, cells were permeabilized with 1% Triton X-100 in PBS (on ice, 2 min), washed with PBS (3×5 min), and then blocked in 5% serum for 1 h. After PBS washing (3×5 min), cells were incubated with primary antibody against NLRP3 (MA5-23919, Thermo Fisher Scientific), and then fluorescence labeled goat-anti-rabbit secondary antibody (ab6717, Abcam, Cambridge, UK) for 1 h. Afterwards, cells were stained with 4',6-diamidino-2-phenylindole (DAPI) for 15 min in the dark before observation under a fluorescence microscope (Olympus Corporation, Japan). Each assay was repeated thrice.

Quantitative reverse transcription-polymerase chain reaction (qRT-PCR)

Total RNA of cells and tissues was extracted by RNeasy Mini Kit (Qiagen, Valencia, CA, USA), and RNA purity and concentration were measured by a Nano Drop spectrophotometer. A RT kit was employed for the acquisition of cDNA. Afterwards, the samples underwent qPCR with the help of SYBR® Premix Ex Taq™ II (Perfect Real Time) kit (DRR081, Takara, Toyko, Japan) and a fluorescence qPCR instrument (ABI 7500, ABI, Foster City, CA, USA). Each sample had 3 replicates. Data were analyzed with the $2^{-\Delta\Delta Ct}$ method, with glyceraldehyde-3-phosphate dehydrogenase (GAPDH) as the normalizer. The PCR primers are detailed as follows: NOX4 (forward: ACCAAATGTTGGGCGATTGTG, reverse: GATGAGGCTGCAGTTGAGGT), NLRP3 (forward: AGGCTGCTATCTGGAGGAACT, reverse: CCTTTCTCGGGCGGGTAATC), and GAPDH (forward: ACCCTTAAGAGGGATGCTGC, reverse: ATCCGTTCACACCGACCTTC).

Western blotting

After trypsin digestion, cells were gathered and then lysed with enhanced protease inhibitor-containing RIPA lysis buffer. Protein-concentration was determined using a bicinchoninic acid protein assay kit (Boster Biological Technology Co., Ltd., Wuhan, China). Protein was separated with 10% sodium dodecyl sulfate separation gel and then transferred onto polyvinylidene fluoride membranes. Subsequent to 2-h blocking with 5% BSA at room temperature, the membranes received overnight (4 ℃) probing with primary antibodies comprising anti-NOX4 (MA5-32090, 1:1,000, Thermo Fisher Scientific), anti-apoptosis-associated speck-like protein containing a C-terminal caspase recruitment domain (ASC) (ab180799, 1:1,000, Abcam), anti-NLRP3 (ab263899, 1:1,000, Abcam), anti-cleaved caspase-1 (#4199, 1:1,000, CST, Beverly, MA, USA), anti-interleukin-1beta (IL-1β) (ab283818, 1:1,000, Abcam), anti-GSDMD (ab219800, 1:2,000, Abcam), and anti-GAPDH (ab8245, 1:5,000, Abcam). After washing, the membranes received 2-h re-probing with horseradish peroxidase labeled secondary antibodies (ab6728 and ab6721, 1:2,000, Abcam). Protein bands were visualized with ECL (P0018FS, Beyotime, Shanghai, China), detected on a chemiluminescent

imaging system (Bio-rad), and then analyzed by Quantity One v4.6.2 software. Three experiments were performed in parallel.

Detection of superoxide dismutase (SOD) activity and malondialdehyde (MDA) content

HL-1 cells were amassed and centrifuged with the supernatant collected, followed by the measurement of SOD activity and MDA content using the SOD (A001-3-2) and MDA (A003-1-2) kits from JianCheng Bioengineering Institute (Nanjing, China). Each assay was repeated thrice.

Glutathione (GSH) measurement

The activity of GSH in cells or tissues was evaluated using the kit (CS0260, Sigma-Aldrich). In brief, cells (1×10^8) were planted onto a plate, washed in PBS, and added with 5-sulfosalicylic acid (SSA) solution (3 vol, 5%). After 10-min centrifugation (10,000 g), the supernatant underwent successive incubation with GSH mixture (150 μL) for 5 min and diluted NADPH solution (50 μL) for 20 min. The absorbance at 412 nm was assessed using a microplate reader.

Animal treatment

Thirty male C57BL/6J mice (20±2 g, 8 weeks old, Beijing Vital River Laboratory Animal Technology Co., Ltd., Beijing, China) were raised in a specific pathogen-free room (21–25°C temperature, 50–65% humidity, and a 12-h light/dark cycle) with free access to food and water. Mice underwent an adaptive feeding for 1 week before the study commenced. Notably, female mice may have some influences on the experimental results due to the influence of estrogen and other hormones, while male mice tend to have more stable hormone levels in their bodies, so we used male mice for our experiment.

The animal experimental operation was ratified by the Ethics Committee of Jiangxi Provincial People's Hospital (No. KT047), in compliance with the guidelines of our hospital for the care and use of animals. The dose and time of DOX treatment in mice were compared with a previous literature (21). Specifically, model mice were intraperitoneally injected with DOX (5 mg/kg), while an equal amount of normal saline (including 0.5% DMSO) was for control mice. The injection was implemented once a week for 5 weeks.

Animal grouping

Mice were distributed into the control group (N=6) and the DOX group (N=24) using random number table method referring to the previous method (22). Mice in the DOX group were subdivided into the following three groups according to different treatments: sh-NC + oe-NC, sh-NOX4 + oe-NC, and sh-NOX4 + oe-NLRP3 groups, with 6 mice in each group. After the 4th injection of DOX, mice in the sh-NOX4 + oe-NC group were injected intravenously with sh-NOX4 and oe-NC adeno-associated viral AAV9 vectors with a titer of $1×10^{12}$ viral genomes (v.g.), while mice in the sh-NOX4 + oe-NLRP3 group were subjected to the injection of sh-NOX4 and oe-NLRP3 vectors ($1×10^{12}$ v.g.). The packaged adeno-associated virus particles were purchased from Hanbio Biotechnology Co., Ltd. (Shanghai, China). Eight weeks after the 1st injection of DOX, Cardiac function was assessed by blinded trial personnel. The stable expression time of adeno-associated viruses in animals is 2 weeks, and it takes a certain amount of time to play a role in reducing DOX induction. Therefore, 8 weeks was selected as the time point to terminate animal experiments by referring to previous literature (21). During 5–8 weeks, the mice did not undergo any treatment as they waited for the adeno-associated virus to take effect. Last, mice were euthanized, and the serum was gathered via tail vein centrifugation and their cardiac tissues were collected for further testing. To ensure the uniformity of the sample size of each group, 2 additional mice were added to each group to supplement the dead or excluded mice. When the remaining number of mice in a group was greater than 6, 6 mice were randomly selected as the final sample size. A total of 2 mice were eliminated during the experiment, including one mouse in the sh-NC + oe-NC group and one mouse in the sh-NOX4 + oe-NLRP3 group, both of which were due to weight loss greater than 20% during the experiment.

Electrocardiogram detection

Mice were anesthetized with 1% isoflurane and kept at constant body temperature with a heating plate, followed by heart rate analysis. The electrodes were placed under the skin of the right hindlimb, right forelimb, and left hindlimb, and the results were recorded by a small animal electrocardiogram machine (BL-420S, Techman Software, Chengdu, China) after the heart rate of the mice stabilized. The duration of each recording was at least 2 min.

Echocardiographic examination

An echocardiographic system (V6, Vinno, China) equipped with 30 MHz probe was adopted for the evaluation of the changes of cardiac function of mice in each group. To be specific, mice were anesthetized with 1% isoflurane and kept at constant body temperature with a heating plate. Next, the limbs of the mice were fixed, and the probe was placed on the left chest coated with the coupling agent, with the detection depth being adjusted to 2.0–2.5 cm. The position of the probe was adjusted to obtain parasternal long-axis B-Mode images so as to clearly display the maximum long-axis section of the left ventricle and measure the structure and systolic function of the left ventricle (23). The indicators included left ventricular ejection fraction (LVEF), left ventricular fractional shortening (LVFS), and left ventricular end-diastolic diameter (LVEDD). The values were averaged over three cardiac cycles.

Assessment of lactic dehydrogenase (LDH), creatine kinase MB (CK-MB), cardiac troponin I (cTnI), and myoglobin

The content of myocardial injury markers (LDH, CK-MB, cTnI, and myoglobin) was detected with corresponding kits [A020-2-2, H197-1-1, and E019-1-1 (JianCheng Bioengineering Institute), and ml092664 (mlbio, Shanghai, China)]. In short, the serum samples were added to a 96-well plate and underwent operations with the manuals of the kits. The optical density (OD) was measured on a microplate reader.

ROS assay

ROS activity in cells and mitochondria was measured as previously described (24). In brief, grouped cells were loaded with 5 μmol/mL of Cell Rox probe (C10444, Thermo Fisher Scientific) or Mito Sox probe (M36008, Thermo Fisher Scientific) for 30 min or 10 min at 37 ℃ in the dark, after which the probes were discarded. Next, the cells fixed by paraformaldehyde (4%, 15 min) were stained by DAPI (1 μg/mL) for 15 min in the dark and then treated with an anti-fluorescence quencher, followed by fluorescence microscope (Olympus Corporation, Japan) observation. The average fluorescence intensity was analyzed by ImageJ software.

To determine the ROS activity in myocardial tissues, the following steps were performed using a ROS kit (mlbio). Specifically, the myocardial tissues were mixed in a certain

amount of PBS solution (pH =7.4), followed by 20-min centrifugation (2,000–3,000 rpm/min). The supernatant was gathered and diluted at a ratio of 1:1. Subsequently, 50 µL samples were added to reaction wells and cultured for 1-h at 37 ℃. Afterwards, the plates were washed for 3 times with 30 s for each time. After color development, 50 µL of stop buffer was dropped immediately, and the OD value of each well was determined at 450 nm wavelength.

Statistical analysis

Statistical analysis of the collected original data was conducted using GraphPad prism7 software, and the processed data were presented as mean ± standard deviation. We used the skewness coefficient and kurtosis coefficient to test the normality of the data, and excluded a small amount of data that do not conform to the normal distribution. *T*-test and one-way analysis of variance were employed for comparisons between two groups and among groups, respectively. Tukey's multiple comparisons test was applied for *post hoc* analysis. Differences were considered to be statistically significant when P<0.05.

Results

NOX4 expression was high in DOX-treated cardiomyocytes

After DOX treatment, we detected HL-1 cell proliferation. The proliferation rate of HL-1 cells decreased significantly with the increase of DOX concentration, reaching approximately 50% upon DOX treatment (5 µmol/L) (*Figure 1A*, P<0.05), displayed by MTT results. Therefore, 5 µmol/L of DOX was selected for subsequent experiments.

Subsequently, we tested the effects of DOX on cardiomyocyte injury and pyroptosis. The results of ROS measurement by CellRox and MitoSox showed that the ROS activity in HL-1 cells and mitochondria was evidently increased in the DOX group versus the control group (*Figure 1B*, P<0.01). In comparison with the control group, the DOX group exhibited higher levels of LDH and MDA, but lower levels of SOD and GSH (*Figure 1C-1F*, P<0.01). Additionally, IF and western blotting results reflected that the expression of NLRP3, ASC, cleaved caspase-1, IL-1β, and GSDMD-NT was obviously elevated in the DOX group (*vs.* the control group) (*Figure 1G,1H*, P<0.05). Furthermore, DOX treatment augmented NOX4 expression in HL-1 cells (*vs.* the control group) (*Figure 1I*, P<0.05). Collectively, DOX treatment could induce cardiomyocyte injury and pyroptosis, and increase NOX4 expression in HL-1 cells.

NOX4 knockdown alleviated DOX-induced cardiomyocyte injury and pyroptosis

To further ascertain the relationship between NOX4 and cardiomyocyte injury and pyroptosis, sh-NOX4 or oe-NOX4 vector was transfected into DOX-induced HL-1 cells, followed by the evaluation of transfection efficiency. NOX4 expression was clearly reduced in the sh-NOX4 group (*vs.* the sh-NC group), but elevated in the oe-NOX4 group (*vs.* the oe-NC group) (*Figure 2A*, P<0.01). Afterwards, the changes in cardiomyocyte injury and pyroptosis were observed. As manifested in *Figure 2B-2G* (P<0.05), the sh-NOX4 group had decreased levels of ROS, LDH, and MDA and increased cell proliferation and the levels of SOD and GSH (*vs.* the sh-NC group). Moreover, the expression of NLRP3, ASC, cleaved caspase-1, IL-1β, and GSDMD-NT was markedly repressed in the sh-NOX4 group versus the sh-NC group (*Figure 2H,2I*, P<0.01). The above results suggested that the knockdown of NOX4 could relieve cardiomyocyte injury and pyroptosis induced by DOX. When the oe-NOX4 group was compared with the oe-NC group, the opposite results were obtained (*Figure 2B-2I*, P<0.05), indicating that overexpression of NOX4 could aggravate cardiomyocyte injury and pyroptosis.
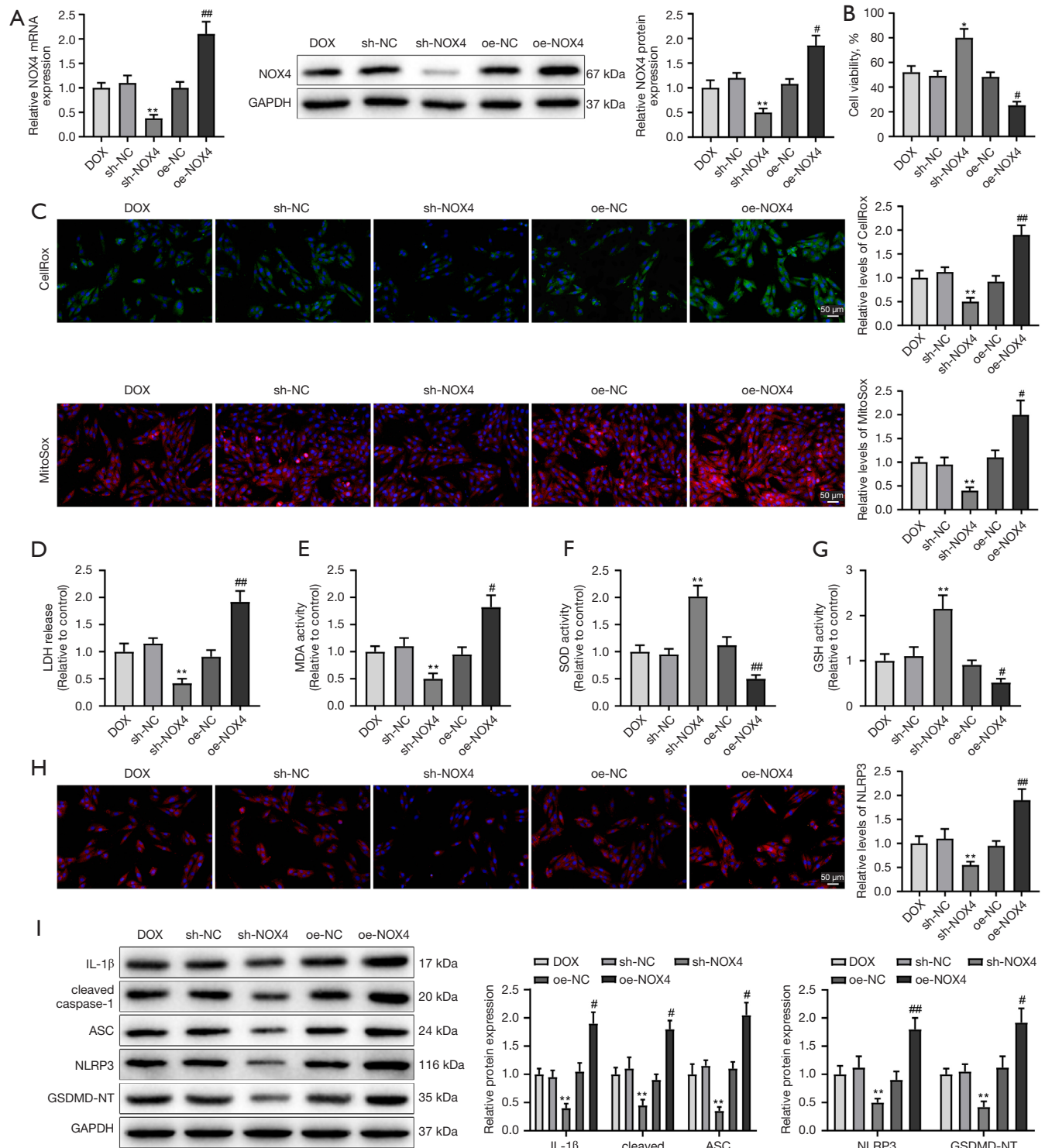
NOX4 exacerbated cardiomyocyte injury and pyroptosis by increasing ROS and NLRP3 expression

Based on the above findings, we assumed that NOX4 mediated ROS accumulation and then activated NLRP3 expression to promote cardiomyocyte injury and pyroptosis. In order to verify our hypothesis, we treated DOX-induced HL-1 cells with oe-NOX4 and NAC simultaneously and then observed the damage degree and pyroptosis of cardiomyocytes.

Compared with the oe-NOX4 + DMSO group, the oe-NOX4 + NAC group had lower ROS activity (*Figure 3A*, P<0.05). Next, we evaluated the expression level of NLRP3. Results showed decreased mRNA and protein expression of NLRP3 in the oe-NOX4 + NAC group versus the oe-NOX4 + DMSO group (*Figure 3B*, P<0.05). As expected, NAC reversed the aggravating effects of NOX4 overexpression on DOX-induced cardiomyocyte injury and pyroptosis (*Figure 3C-3I*, P<0.05). In conclusion, NOX4 elevated ROS production to increase NLRP3 expression,
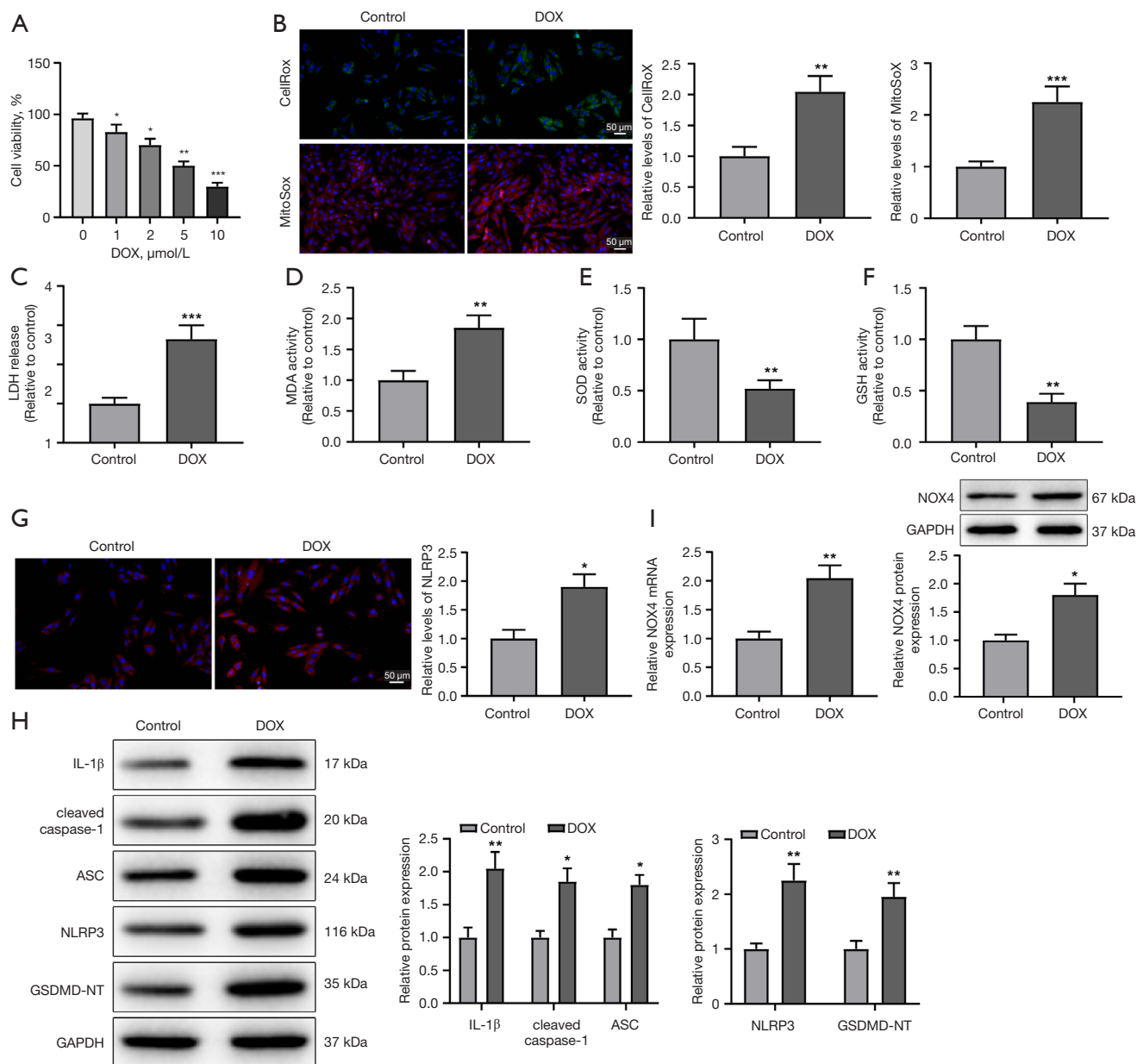
Figure 1 NOX4 is upregulated in DOX-treated cardiomyocytes. (A) HL-1 cell proliferation was tested by MTT assay after treatment with different concentrations of DOX. After DOX treatment (5 µmol/L); (B) the activity of ROS in HL-1 cells and mitochondria was measured by CellRox and MitoSox probes; (C-F) the levels of LDH, MDA, SOD, and GSH were examined by kits; (G) IF was used to detect the expression of NLRP3; (H) the protein expression of NLRP3, ASC, cleaved caspase-1, IL-1β, and GSDMD-NT was detected by western blotting; (I) NOX4 expression was tested by qRT-PCR and western blotting. Data were expressed as mean ± standard deviation, and each experiment was repeated thrice. *, P<0.05 ; **, P<0.01; ***, P<0.001, compared with the control group. DOX, doxorubicin; LDH, lactic dehydrogenase; MDA, malondialdehyde; IF, immunofluorescence; ROS, reactive oxygen species; SOD, superoxide dismutase; GSH, glutathione; NOX4, nicotinamide adenine dinucleotide phosphate oxidase 4; NLRP3, nucleotide-binding and oligomerization domain-like receptor protein 3; MTT, 3-(4,5-dimethylthiazol-2-yl)-2,5-diphenyltetrazolium bromide; qRT-PCR, quantitative reverse transcription-polymerase chain reaction; IL-1β, interleukin-1beta.

Figure 2 Overexpressed NOX4 aggravates cardiomyocyte injury and pyroptosis. After DOX-induced HL-1 cells were transfected with sh-NOX4 or oe-NOX4, (A) qRT-PCR and western blotting were used to detect the expression of NOX4; (B) cell proliferation was measured by MTT assay; (C) the activity of ROS in HL-1 cells and mitochondria was tested by CellRox and MitoSox probes; (D-G) the levels of LDH, MDA, SOD, and GSH were examined by kits; (H) the expression of NLRP3 was measured by IF; (I) the protein expression of NLRP3, ASC, cleaved caspase-1, IL-1β, and GSDMD-NT was detected by western blot. Data were exhibited as mean ± standard deviation, and each assay was repeated three times. *, P<0.05;

**, P<0.01, compared with the sh-NC group; #, P<0.05, ##, P<0.01, compared with the oe-NC group. NOX4, nicotinamide adenine dinucleotide phosphate oxidase 4; DOX, doxorubicin; LDH, lactic dehydrogenase; MDA, malondialdehyde; SOD, superoxide dismutase; GSH, glutathione; NLRP3, nucleotide-binding and oligomerization domain-like receptor protein 3; IL-1β, interleukin-1beta; MTT, 3-(4,5-dimethylthiazol-2-yl)-2,5-diphenyltetrazolium bromide; qRT-PCR, quantitative reverse transcription-polymerase chain reaction; ROS, reactive oxygen species; IF, immunofluorescence.
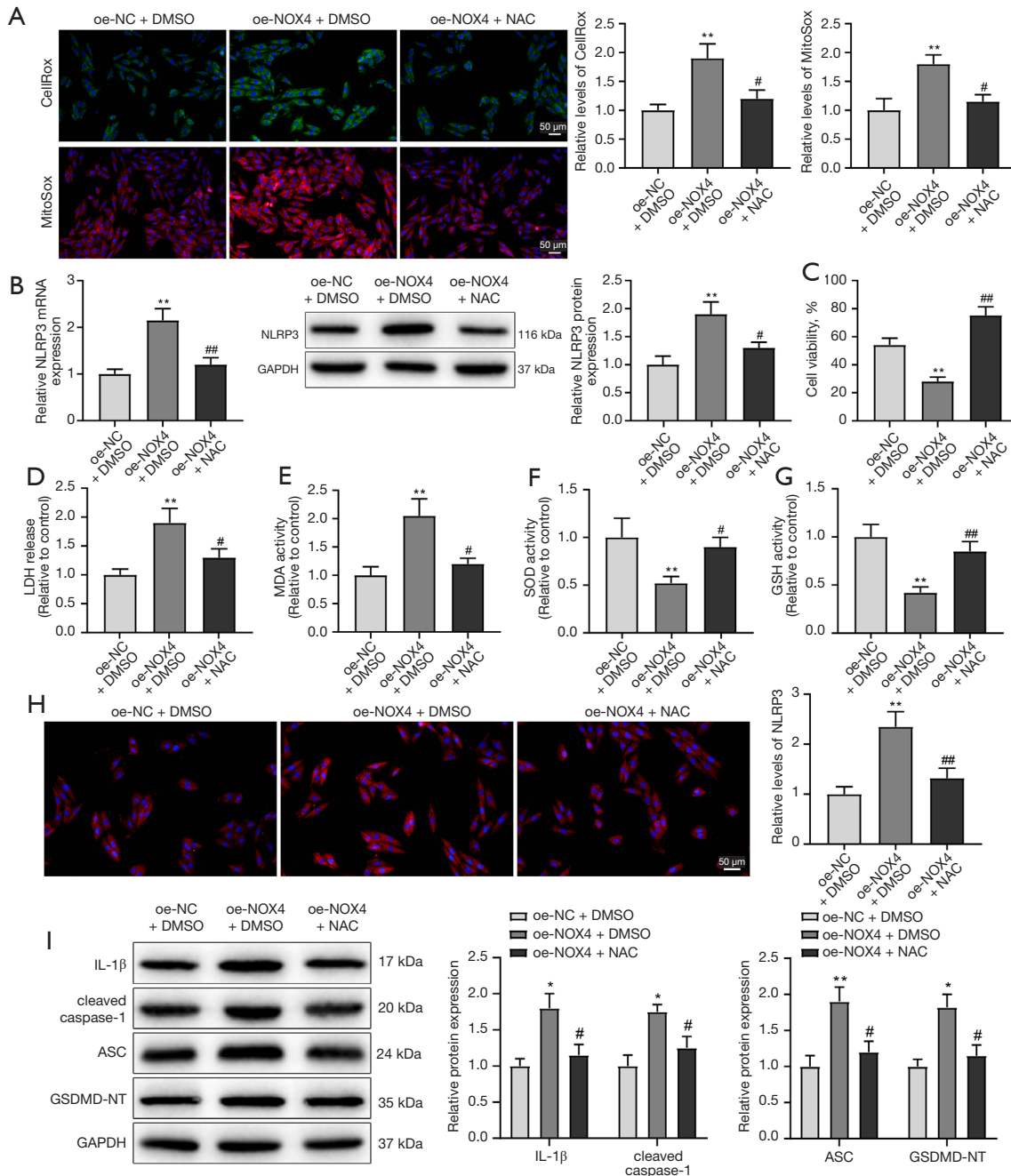
Figure 3 NOX4 affects cardiomyocyte injury and pyroptosis via regulating ROS and NLRP3 levels. After DOX-induced HL-1 cells were treated with oe-NOX4 and NAC, (A) CellRox and MitoSox probes were used to detect the activity of ROS; (B) the expression of NLRP3 was measured by qRT-PCR and western blotting; (C) MTT was used to evaluate cell proliferation; (D-G) the levels of LDH, MDA, SOD, and GSH were assessed by kits;

(H) the expression of NLRP3 was tested by IF; (I) the protein expression of ASC, cleaved caspase-1, IL-1β, and GSDMD-NT was measured by western blotting. Data were expressed in the form of mean ± standard deviation, and each assay was conducted in triplicate. *, P<0.05; **, P<0.01, compared with the oe-NC + DMSO group; #, P<0.05, ##, P<0.01, compared with the oe-NOX4 + DMSO group. DMSO, dimethylsulfoxide; NAC, N-acetyl-cysteine; NOX4, nicotinamide adenine dinucleotide phosphate oxidase 4; NLRP3, nucleotide-binding and oligomerization domain-like receptor protein 3; LDH, lactic dehydrogenase; MDA, malondialdehyde; SOD, superoxide dismutase; GSH, glutathione; DOX, doxorubicin; ROS, reactive oxygen species; IF, immunofluorescence; MTT, 3-(4,5-dimethylthiazol-2-yl)-2,5-diphenyltetrazolium bromide; qRT-PCR, quantitative reverse transcription-polymerase chain reaction; IL-1β, interleukin-1beta.

ultimately aggravating DOX-induced cardiomyocyte injury and pyroptosis.

Knockdown of NOX4 mediated ROS production to mitigate DOX-induced cardiomyocyte injury and pyroptosis through NLRP3

To further confirm the relationship between NOX4 and NLRP3, we treated DOX-induced HL-1 cells with sh-NOX4 and oe-NLRP3 vectors. As displayed in *Figure 4A* (P<0.01), NLRP3 expression was distinctly stimulated in the sh-NOX4 + oe-NLRP3 group versus the sh-NOX4 + oe-NC group. Moreover, NLRP3 overexpression reversed the mitigation effect of NOX4 knockdown on DOX-induced cardiomyocyte injury and pyroptosis (*Figure 4B-4I*, P<0.05). Taken together, NOX4 knockdown-mediated reduction in ROS production remitted cardiomyocyte injury and pyroptosis via downregulation of NLRP3.

NOX4 modulated DOX-induced myocardial histopathological changes in mice via ROS/NLRP3

Subsequent to cellular experiments, we injected sh-NOX4 + oe-NC or sh-NOX4 + oe-NLRP3 into DOX-treated mice. Results of qRT-PCR and western blotting revealed that DOX treatment resulted in elevated expression of NOX4 and NLRP3 (*vs.* the control group) (*Figure 5A*, P<0.01). Echocardiographic examination for evaluation of cardiac dysfunction changes indicated that DOX treatment caused increased heart weight/body weight ratio, and LVEDD, and decreased heart rate, LVEF, and LVFS (*vs.* the control group) (*Figure 5B-5G*, P<0.05). However, sh-NOX4 reduced the expression of NOX4 and NLRP3, and memorably alleviated the myocardial histopathological changes induced by DOX in mice compared with the sh-NC + oe-NC group (*Figure 5A-5G*, P<0.05). The myocardial histopathological changes were exacerbated and NLRP3 expression was elevated in the sh-NOX4 + oe-NLRP3 group (*vs.* the sh-

NOX4 + oe-NC group), while there was no clear difference in the expression of NOX4 (*Figure 5A-5G*, P<0.05). It was concluded that NOX4-mediated ROS production could regulate DOX-induced myocardial histopathological changes in mice through NLRP3.

NOX4 deficiency reduces DOX-induced myocardial injury and pyroptosis in vivo via ROS/NLRP3

Subsequently, we detected the effect of sh-NOX4 and/or oe-NLRP3 on DOX-induced myocardial injury and pyroptosis in mice. First, the results of ROS determination manifested that DOX treatment increased the ROS activity (*vs.* the control group) (*Figure 6A*, P<0.001). Also, DOX treatment signally elevated the content of LDH, cTnI, myoglobin, and CK-MB (*vs.* the control group) (*Figure 6B-6E*, P<0.01), accompanied by the increased expression of ASC, cleaved caspase-1, IL-1β, and GSDMD-NT (*Figure 6F*, P<0.01). Related to the sh-NC + oe-NC group, sh-NOX4 treatment markedly reduced myocardial tissue damage caused by DOX and inhibited ROS production and the expression of pyroptosis proteins (*Figure 6A-6F*, P<0.05). The combination treatment of sh-NOX4 and oe-NLRP3 reversed the inhibitory effects of sh-NOX4 alone on myocardial injury and pyroptosis in mice (*Figure 6A-6F*, P<0.05). Overall, NOX4-mediated ROS production regulated DOX-induced myocardial injury and pyroptosis via NLRP3 *in vivo*.

Discussion

As an effective and widely used anticancer drug, DOX exerts anti-tumor effects by promoting gene expression and viral progeny replication, providing a theoretical basis for oncolytic virus therapy and chemotherapy (25). Notably, DOX can also induce myocardial injury, which usually limits its use in chemotherapy for malignant tumors (26). Hence, probing more molecular mechanisms mediating
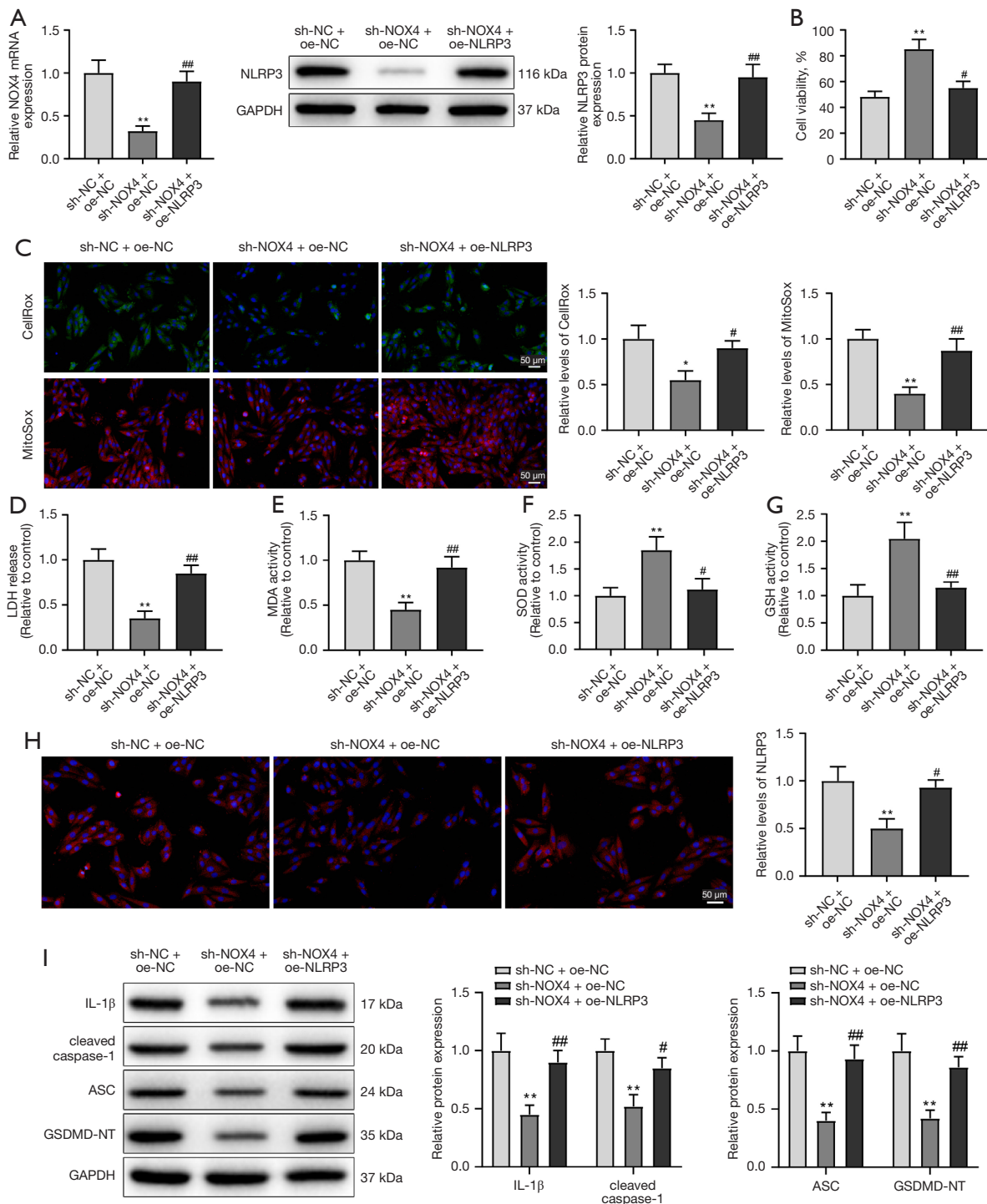
Figure 4 Knockdown of NOX4 eases cardiomyocyte injury and pyroptosis by decreasing ROS and NLRP3 levels. After DOX-induced HL-1 cells were transfected with sh-NOX4 and oe-NLRP3, (A) the expression of NLRP3 was detected by qRT-PCR and western blotting; (B) MTT was used to measure cell proliferation; (C) cellRox and MitoSox probes were used to detect the activity of ROS; (D-G) the levels of LDH, MDA, SOD, and GSH were assessed by kits; (H) the expression of NLRP3 was tested by IF; (I) the protein expression of ASC, cleaved caspase-1, IL-1β, and GSDMD-NT was measured by western blotting. Data were displayed as mean ± standard deviation, and each experiment was run in triplicate. *, P<0.05; **, P<0.01, compared with the sh-NC + oe-NC group; #, P<0.05; ##, P<0.01, compared with the

sh-NOX4 + oe-NC group. NLRP3, nucleotide-binding and oligomerization domain-like receptor protein 3; NOX4, nicotinamide adenine dinucleotide phosphate oxidase 4; DOX, doxorubicin; IF, immunofluorescence; LDH, lactic dehydrogenase; MDA, malondialdehyde; SOD, superoxide dismutase; GSH, glutathione; MTT, 3-(4,5-dimethylthiazol-2-yl)-2,5-diphenyltetrazolium bromide; qRT-PCR, quantitative reverse transcription-polymerase chain reaction; IL-1β, interleukin-1beta; ROS, reactive oxygen species.
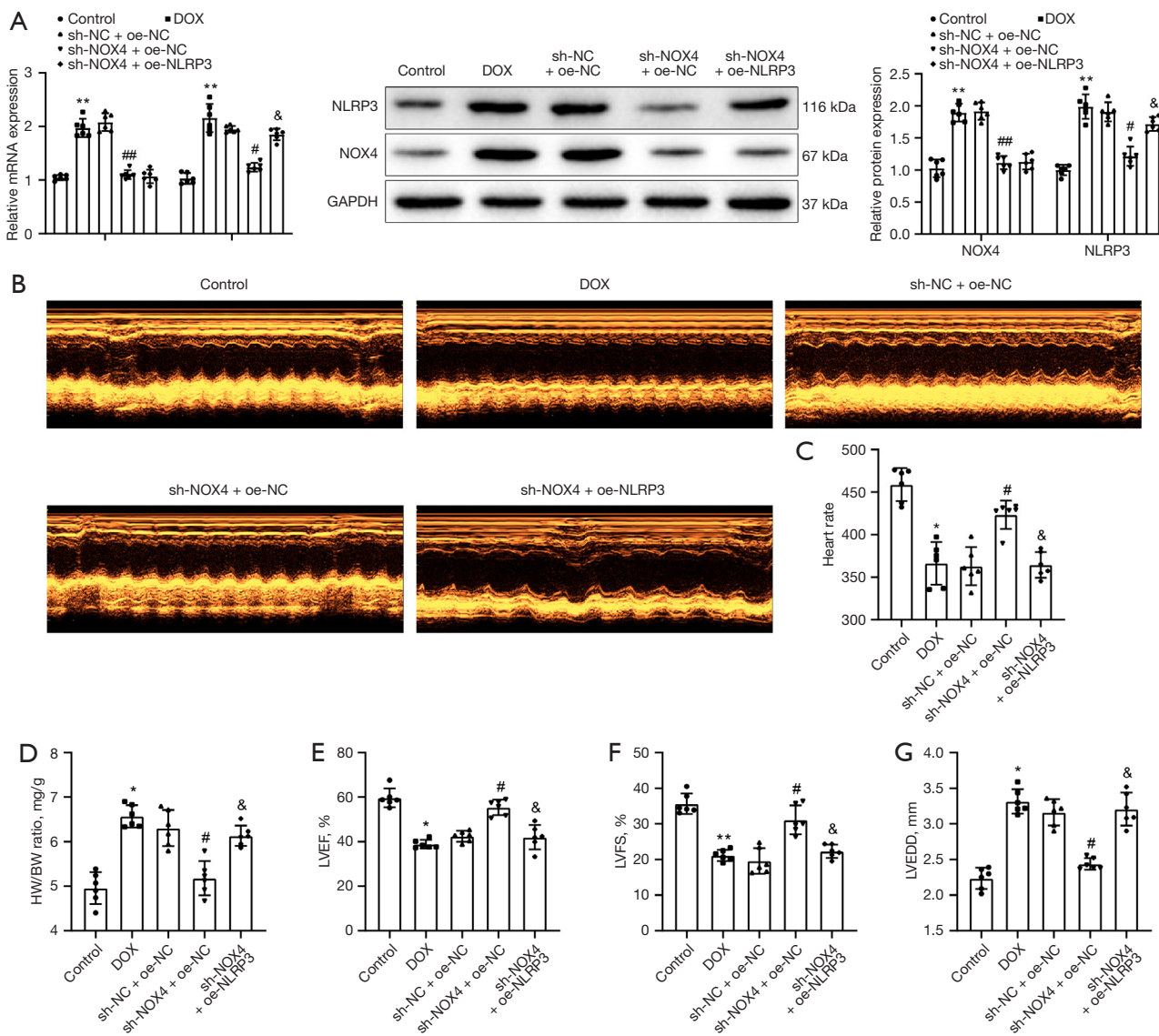
Figure 5 The effect of NOX4/ROS/NLRP3 on DOX-induced myocardial histopathological changes in mice. After the injection of sh-NOX4 + oe-NC or sh-NOX4 + oe-NLRP3 into DOX-treated mice, (A) the expression of NOX4 and NLRP3 was measured by qRT-PCR and western blotting; (B) echocardiographic examination was used for evaluation of cardiac dysfunction changes; (C-G) the heart rate, the heart weight/body weight ratio, LVEF, LVFS, and LVEDD were tested. Data were represented as mean ± standard deviation, N=6 for each group. *, P<0.05; **, P<0.01, compared with the control group; #, P<0.05; ##, P<0.01, compared with the sh-NC + oe-NC group; &, P<0.05, compared with the sh-NOX4 + oe-NC group. DOX, doxorubicin; NOX4, nicotinamide adenine dinucleotide phosphate oxidase 4; NLRP3, nucleotide-binding and oligomerization domain-like receptor protein 3; ROS, reactive oxygen species; HW/BW, heart weight/body weight; LVEF, left ventricular ejection fraction; LVFS, left ventricular fractional shortening; LVEDD, left ventricular end diastolic diameter; H&E, hematoxylin-eosin; qRT-PCR, quantitative reverse transcription-polymerase chain reaction.
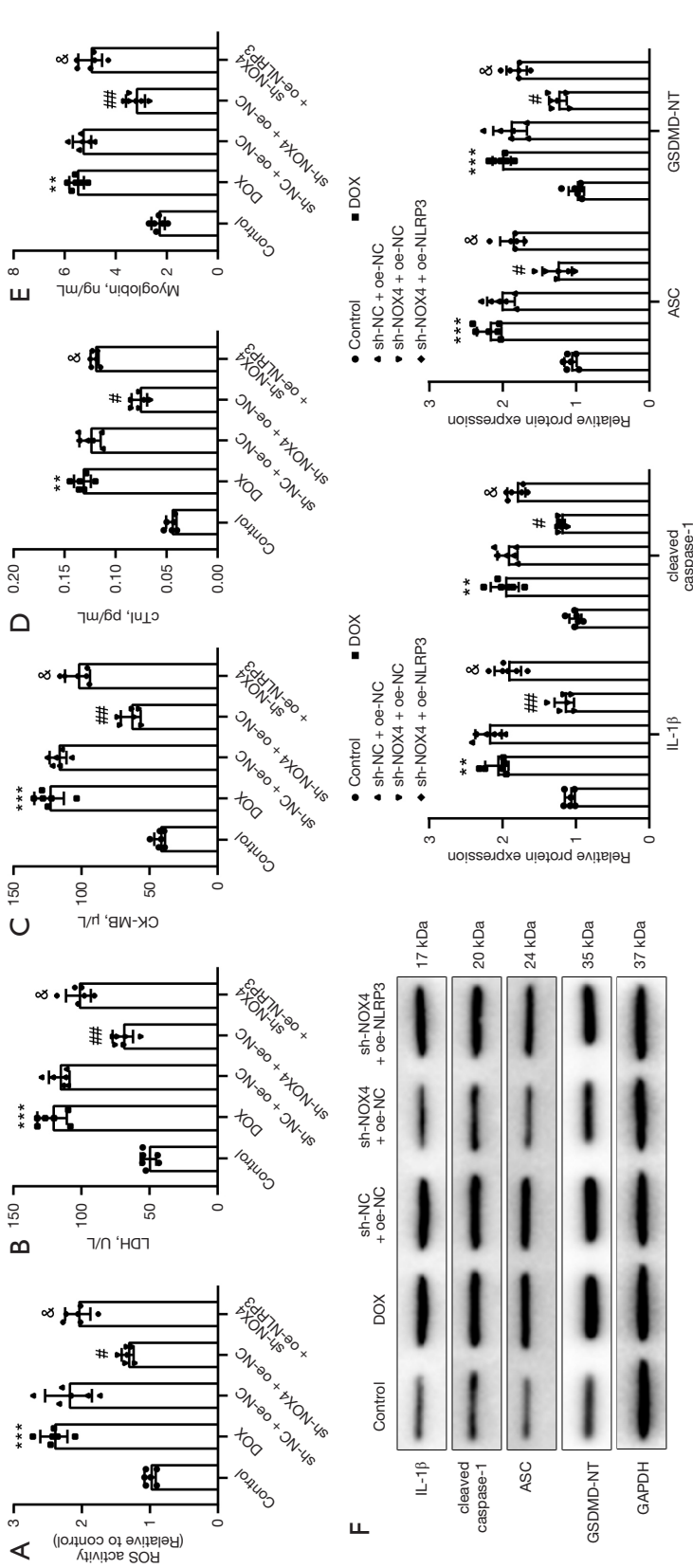
Figure 6 NOX4-mediated ROS accumulation modulates DOX-induced myocardial injury and pyroptosis through NLRP3 *in vivo*. (A) The activity of ROS was measured by a kit; (B-E) the content of LDH, cTnI, myoglobin, and CK-MB was tested by kits. (F) Western blotting was used to examine the protein expression of ASC, cleaved caspase-1, IL-1β, and GSDMD-NT. Data were represented as mean ± standard deviation, N=6 for each group. **, P<0.01, ***, P<0.001, compared with the control group; #, P<0.05, ##, P<0.01, compared with the sh-NC + oe-NC group; &, P<0.05, compared with the sh-NOX4 + oe-NC group. ROS, reactive oxygen species; DOX, doxorubicin; NOX4, nicotinamide adenine dinucleotide phosphate oxidase 4; NLRP3, nucleotide-binding and oligomerization domain-like receptor protein 3; LDH, lactic dehydrogenase; CK-MB, creatine kinase MB; cTnI, cardiac troponin I; IL-1β, interleukin-1beta.

cardiomyocyte function is critical. In the present study, we used DOX to treat HL-1 cells and found that DOX treatment caused cardiomyocyte injury and pyroptosis, and NOX4 and NLRP3 were dramatically augmented in DOX-induced HL-1 cells. Follow-up experiments attested that repressing NOX4 enhanced ROS level and NLRP3 expression to ameliorate myocardial tissue or cell injury and pyroptosis *in vitro* and *in vivo*.

Reportedly, NOX4 is involved in the regulation of a variety of cardiovascular diseases, including atherosclerosis (27), hypertension (28), and heart failure (29), and moreover, its expression was increased in tissues affected in these diseases. At first, in DOX-induced HL-1 cells, NOX4 and NLRP3 were tested to be upregulated. Consistently, Cheng *et al.* found NOX4 was increased in H9C2 cardiomyocytes treated by DOX (30). NOX4 is the main source of cardiac oxygen free radical production, which plays important roles in the growth and death of cardiomyocytes (31). A previous study showed that inhibition of NOX4 could suppress DOX-induced NLPR3 inflammasome activation and cardiomyocyte pyroptosis (9). In addition, NOX4 inhibited by metformin could decrease myocardial oxidative damage and apoptosis, alleviating reperfusion injury (32). In the present study, we observed that low expression of NOX4 significantly attenuated cardiomyocyte injury and pyroptosis after DOX treatment; however, an opposite result was obtained after NOX4 overexpression. As displayed in an existing study, ROS production in DOX-treated H9C2 cells was markedly promoted by overexpressing NOX4 (33). Furthermore, it was well known that the production of ROS was one of the signals to activate NLRP3 inflammasome (34). Based on these previous findings, we hypothesized that NOX4 mediated ROS accumulation and activated NLRP3 inflammasome to expedite cardiomyocyte injury and pyroptosis. Results from further cellular experiments demonstrated that overexpression of NOX4 aggravated cell injury and pyroptosis of DOX-induced HL-1 cells by increasing the ROS content and the expression of NLRP3. On the contrary, the knockdown of NOX4 eased cardiomyocyte injury and pyroptosis via ROS and NLRP3.

ROS is a highly reactive compound with an extremely short half-life, serving as byproducts of numerous enzymatic reactions (35). The moderation of intracellular ROS activity promoted cell proliferation and differentiation, and the over-production of ROS could lead to cytotoxicity (36). Moreover, elevated levels of mitochondrial ROS contributed to the development of numerous cardiovascular diseases (37). For instance, a prior research demonstrated that ROS generation promoted the development and progression of diabetic cardiomyopathy (38). Another study specifically explained that high levels of ROS exerted its aggravation effect in diabetic cardiomyopathy by flowing into the cytoplasm and binding to NLRP3 to activate the NLRP3 inflammasome (39). More importantly, increased ROS was verified to induce NLRP3 inflammasome-mediated pyroptosis, ultimately aggravating high glucose- and hypoxia/reoxygenation-induced H9C2 cell injury (40). According to previous research, ROS/NLRP3 inflammasome signaling pathway was widely studied in myocardial injury. Research by Wei *et al.* highlighted the crucial role of ROS/NLRP3-associated inflammasome activation in DOX-induced cardiotoxicity (41). Additionally, uric acid increased myocardial ischemia-reperfusion-induced activation of the NLRP3 inflammatory cascade and pyroptosis by promoting ROS production (42). In addition to cellular experiments, we also conducted animal experiments and found that NOX4-mediated ROS accumulation regulated DOX-induced myocardial histopathology in mice through NLRP3 inflammasome.

Limitations

In the present work, we set up cell and animal experiments in the study to make our results more convincing. However, the limited sample size and data volume were also the limitations of our experiment. More comprehensive investigations about the regulatory mechanism of NOX4 in DOX-induced myocardial injury and pyroptosis need to be further explored. In addition, the standard practice of Masson trichrome staining was not used in the present study to evaluate myocardial remodeling, which is also an area that needs special attention and improvement in our subsequent studies. In our cell experiment, the design of the control group was not strictly carried out, so that our data lacked a certain rigor. Therefore, more studies and data are needed to support our results in the follow-up study.

Conclusions

In conclusion, this paper confirmed that the knockdown of NOX4 alleviated myocardial injury and pyroptosis following DOX induction through ROS/NLRP3 inflammasome signaling pathway. Our findings may provide potential clinical therapeutic targets for reducing DOX-induced myocardial injury.

Footnote

Reporting Checklist: The authors have completed the ARRIVE reporting checklist. Available at https://cdt.amegroups.com/article/view/10.21037/cdt-23-142/rc

Data Sharing Statement: Available at https://cdt.amegroups.com/article/view/10.21037/cdt-23-142/dss

Peer Review File: Available at https://cdt.amegroups.com/article/view/10.21037/cdt-23-142/prf

Conflicts of Interest: All authors have completed the ICMJE uniform disclosure form (available at https://cdt.amegroups.com/article/view/10.21037/cdt-23-142/coif). L.S. reports that this study was funded by the National Natural Science Foundation of China (No. 82160053; No. 82260078). The other authors have no conflicts of interest to declare.

Ethical Statement: The authors are accountable for all aspects of the work in ensuring that questions related to the accuracy or integrity of any part of the work are appropriately investigated and resolved. The animal experimental operation was ratified by the Ethics Committee of Jiangxi Provincial People's Hospital (approval No. KT047), in compliance with the guidelines of our hospital for the care and use of animals.

References

1. Zhao H, Yu J, Zhang R, et al. Doxorubicin prodrug-based nanomedicines for the treatment of cancer. Eur J Med Chem 2023;258:115612.
2. Sawicki KT, Sala V, Prever L, et al. Preventing and Treating Anthracycline Cardiotoxicity: New Insights. Annu Rev Pharmacol Toxicol 2021;61:309-32.
3. Ji N, Qi Z, Wang Y, et al. Pyroptosis: A New Regulating Mechanism in Cardiovascular Disease. J Inflamm Res 2021;14:2647-66.
4. Shi S, Chen Y, Luo Z, et al. Role of oxidative stress and inflammation-related signaling pathways in doxorubicin-induced cardiomyopathy. Cell Commun Signal 2023;21:61.
5. Chen Y, Shi S, Dai Y. Research progress of therapeutic drugs for doxorubicin-induced cardiomyopathy. Biomed Pharmacother 2022;156:113903.
6. Zhang L, Fan C, Jiao HC, et al. Calycosin Alleviates Doxorubicin-Induced Cardiotoxicity and Pyroptosis by Inhibiting NLRP3 Inflammasome Activation. Oxid Med Cell Longev 2022;2022:1733834.
7. Kesavardhana S, Malireddi RKS, Kanneganti TD. Caspases in Cell Death, Inflammation, and Pyroptosis. Annu Rev Immunol 2020;38:567-95.
8. Zhaolin Z, Guohua L, Shiyuan W, et al. Role of pyroptosis in cardiovascular disease. Cell Prolif 2019;52:e12563.
9. Zeng C, Duan F, Hu J, et al. NLRP3 inflammasome-mediated pyroptosis contributes to the pathogenesis of non-ischemic dilated cardiomyopathy. Redox Biol 2020;34:101523.
10. Pecchillo Cimmino T, Ammendola R, Cattaneo F, et al. NOX Dependent ROS Generation and Cell Metabolism. Int J Mol Sci 2023;24:2086.
11. Ni Y, Zhang J, Zhu W, et al. Echinacoside inhibited cardiomyocyte pyroptosis and improved heart function of HF rats induced by isoproterenol via suppressing NADPH/ROS/ER stress. J Cell Mol Med 2022;26:5414-25.
12. Chen A, Chen Z, Xia Y, et al. Liraglutide attenuates NLRP3 inflammasome-dependent pyroptosis via regulating SIRT1/NOX4/ROS pathway in H9c2 cells. Biochem Biophys Res Commun 2018;499:267-72.
13. Tang YS, Zhao YH, Zhong Y, et al. Neferine inhibits LPS-ATP-induced endothelial cell pyroptosis via regulation of ROS/NLRP3/Caspase-1 signaling pathway. Inflamm Res 2019;68:727-38.
14. Zhang Y, Liu Q, Yin H, et al. Cadmium exposure induces pyroptosis of lymphocytes in carp pronephros and spleens by activating NLRP3. Ecotoxicol Environ Saf 2020;202:110903.
15. Wang X, Bian Y, Zhang R, et al. Melatonin alleviates cigarette smoke-induced endothelial cell pyroptosis

through inhibiting ROS/NLRP3 axis. Biochem Biophys Res Commun 2019;519:402-8.

16. Xiao Z, Yu Z, Chen C, et al. GAS-STING signaling plays an essential pathogenetic role in Doxorubicin-Induced Cardiotoxicity. BMC Pharmacol Toxicol 2023;24:19.

17. Zhang WC, Yang JH, Liu GH, et al. miR-34b/c regulates doxorubicin-induced myocardial cell injury through ITCH. Cell Cycle 2019;18:3263-74.

18. Guo L, Zheng X, Wang E, et al. Irigenin treatment alleviates doxorubicin (DOX)-induced cardiotoxicity by suppressing apoptosis, inflammation and oxidative stress via the increase of miR-425. Biomed Pharmacother 2020;125:109784.

19. Chen H, Li S, Yin H, et al. MYC-mediated miR-320a affects receptor activator of nuclear factor κB ligand (RANKL)-induced osteoclast formation by regulating phosphatase and tensin homolog (PTEN). Bioengineered 2021;12:12677-87.

20. Ko J, Kang HJ, Kim DA, et al. Paricalcitol attenuates TGF-β1-induced phenotype transition of human peritoneal mesothelial cells (HPMCs) via modulation of oxidative stress and NLRP3 inflammasome. FASEB J 2019;33:3035-50.

21. Qi Y, Chen J, Duan J, et al. Major vault protein attenuates cardiomyocyte injury in doxorubicin-induced cardiomyopathy through activating AKT. BMC Cardiovasc Disord 2022;22:77.

22. Wang A J, Tang Y, Zhang J, et al. Cardiac SIRT1 ameliorates doxorubicin-induced cardiotoxicity by targeting sestrin 2. Redox Biol 2022;52:102310.

23. Wang X, Ye Y, Gong H, et al. The effects of different angiotensin II type 1 receptor blockers on the regulation of the ACE-AngII-AT1 and ACE2-Ang(1-7)-Mas axes in pressure overload-induced cardiac remodeling in male mice. J Mol Cell Cardiol 2016;97:180-90.

24. Leng Y, Wu Y, Lei S, et al. Inhibition of HDAC6 Activity Alleviates Myocardial Ischemia/Reperfusion Injury in Diabetic Rats: Potential Role of Peroxiredoxin 1 Acetylation and Redox Regulation. Oxid Med Cell Longev 2018;2018:9494052.

25. Xiao B, Ying C, Chen Y, et al. Doxorubicin hydrochloride enhanced antitumour effect of CEA-regulated oncolytic virotherapy in live cancer cells and a mouse model. J Cell Mol Med 2020;24:13431-9.

26. Tadokoro T, Ikeda M, Ide T, et al. Mitochondria-dependent ferroptosis plays a pivotal role in doxorubicin cardiotoxicity. JCI Insight 2023;8:e169756.

27. Yu W, Li S, Wu H, et al. Endothelial Nox4 dysfunction

aggravates atherosclerosis by inducing endoplasmic reticulum stress and soluble epoxide hydrolase. Free Radic Biol Med 2021;164:44-57.

28. Guo X, Fan Y, Cui J, et al. NOX4 expression and distal arteriolar remodeling correlate with pulmonary hypertension in COPD. BMC Pulm Med 2018;18:111.

29. Zhong Z, Tian Y, Luo X, et al. Extracellular Vesicles Derived From Human Umbilical Cord Mesenchymal Stem Cells Protect Against DOX-Induced Heart Failure Through the miR-100-5p/NOX4 Pathway. Front Bioeng Biotechnol 2021;9:703241.

30. Cheng D, Tu W, Chen L, et al. MSCs enhances the protective effects of valsartan on attenuating the doxorubicin-induced myocardial injury via AngII/NOX/ROS/MAPK signaling pathway. Aging (Albany NY) 2021;13:22556-70.

31. Chen X, Xu S, Zhao C, et al. Role of TLR4/NADPH oxidase 4 pathway in promoting cell death through autophagy and ferroptosis during heart failure. Biochem Biophys Res Commun 2019;516:37-43.

32. Shi Y, Hou SA. Protective effects of metformin against myocardial ischemia-reperfusion injury via AMPK-dependent suppression of NOX4. Mol Med Rep 2021;24:712.

33. Cheng D, Chen L, Tu W, et al. Protective effects of valsartan administration on doxorubicin-induced myocardial injury in rats and the role of oxidative stress and NOX2/NOX4 signaling. Mol Med Rep 2020;22:4151-62.

34. Liao Y, Lin X, Li J, et al. Nodakenin alleviates renal ischaemia-reperfusion injury via inhibiting reactive oxygen species-induced NLRP3 inflammasome activation. Nephrology (Carlton) 2021;26:78-87.

35. Forrester SJ, Kikuchi DS, Hernandes MS, et al. Reactive Oxygen Species in Metabolic and Inflammatory Signaling. Circ Res 2018;122:877-902.

36. Luo Z, Xu X, Sho T, et al. ROS-induced autophagy regulates porcine trophectoderm cell apoptosis, proliferation, and differentiation. Am J Physiol Cell Physiol 2019;316:C198-209.

37. Incalza MA, D'Oria R, Natalicchio A, et al. Oxidative stress and reactive oxygen species in endothelial dysfunction associated with cardiovascular and metabolic diseases. Vascul Pharmacol 2018;100:1-19.

38. Kaludercic N, Di Lisa F. Mitochondrial ROS Formation in the Pathogenesis of Diabetic Cardiomyopathy. Front Cardiovasc Med 2020;7:12.

39. Zhang H, Chen X, Zong B, et al. Gypenosides improve

diabetic cardiomyopathy by inhibiting ROS-mediated NLRP3 inflammasome activation. J Cell Mol Med 2018;22:4437-48.

40. Qiu Z, He Y, Ming H, et al. Lipopolysaccharide (LPS) Aggravates High Glucose- and Hypoxia/Reoxygenation-Induced Injury through Activating ROS-Dependent NLRP3 Inflammasome-Mediated Pyroptosis in H9C2 Cardiomyocytes. J Diabetes Res 2019;2019:8151836.

41. Wei S, Ma W, Li X, et al. Involvement of ROS/NLRP3 Inflammasome Signaling Pathway in Doxorubicin-Induced Cardiotoxicity. Cardiovasc Toxicol 2020;20:507-19.

42. Shen S, He F, Cheng C, et al. Uric acid aggravates myocardial ischemia-reperfusion injury via ROS/NLRP3 pyroptosis pathway. Biomed Pharmacother 2021;133:110990.